Published in "Physical Review B 78(09): 094302, 2008"
which should be cited to refer to this work.

Dynamical properties and temperature induced molecular disordering of $LiBH_4$ and $LiBD_4$

F. Buchter,* Z. Łodziana, Ph. Mauron, A. Remhof, O. Friedrichs, A. Borgschulte, and A. Züttel†
EMPA, Swiss Federal Laboratories for Materials Testing and Research, Laboratory for Hydrogen & Energy, Überlandstrasse 129, CH-8600 Dübendorf, Switzerland

D. Sheptyakov and Th. Strässle
Laboratory for Neutron Scattering, ETH Zurich & Paul Scherrer Institut, CH-5232 Villigen PSI, Switzerland

A. J. Ramirez-Cuesta
ISIS Facility, Rutherford Appleton Laboratory, Chilton, Didcot, Oxon OX11 0QX, United Kingdom

We report on neutron powder-diffraction experiments, inelastic incoherent neutron-scattering experiments, and density-functional calculations on dynamics, order and disorder properties of $LiBH_4$ and $LiBD_4$. From refinement of $LiBD_4$ structure at 10 and 302 K, we found an almost ideal tetrahedral geometry of BD_4 ions (difference between shortest and longest interatomic distances is less than 4% for B-D bond, and less than 3% for D-D bond), close to the calculated geometry. A quantitative agreement was found between experimental and calculated anisotropic temperature factors of individual atoms. For phonon energies <15 meV, the phonon density of states of $LiBH_4$ in the low-temperature phase depends quadratically on the phonon energy while for the high-temperature phase a linear dependence is observed, revealing a high lattice anharmonicity in the high-temperature phase. Moreover, an increased phonon density of states at low energies in the high-temperature phase compared to the low-temperature phase give a direct evidence for disorder in the high-temperature phase of $LiBH_4$ of the hydrogen sublattice which can originate from orientational disorder of BH_4 units. Potential energy landscape for rotation of BH_4 indicates that fairly localized minima and barriers higher than 0.6 eV exist in the low-temperature phase, i.e., ordered BH_4 ions. The high-temperature structure shows shallow barriers of ~ 0.2 eV without distinct energy minima, i.e., orientation of a single BH_4 unit cannot be precisely defined. This corroborates the large thermal displacements observed in diffraction studies and high disorder of BH_4 ions deduced from experimental partial phonon density of states in the high-temperature phase.

DOI: 10.1103/PhysRevB.78.094302 PACS number(s): 63.50.Gh, 63.70.+h, 29.30.Hs, 61.66.Dk

I. INTRODUCTION

Alkali and earth alkali complex hydrides have attracted a growing interest as hydrogen storage materials.[1–3] Their applicability is due to their high gravimetric density of hydrogen up to 20 mass% and high volumetric density up to 150 kg m^{-3}. For practical use, these compounds require reversible hydrogen release and uptake at temperature/pressure conditions reasonably close to the ambient ones. Unfortunately, not all these requirements are fulfilled by any simple alkali or earth alkali complex hydride, due to either thermodynamic or kinetic reasons.[1–3] Limiting kinetics can in principle be enhanced, by use of an appropriate catalyst [e.g., Ti or Ti compounds for $NaAlH_4$ (Refs. 2 and 4)]. However, elevated decomposition temperatures due to thermodynamical limitations cannot be influenced by a catalyst. Therefore, before addressing kinetics of hydrogen desorption and uptake, it is crucial to find compounds with appropriate thermodynamic stability, for the pressure and temperature conditions required for practical use.[1–3,5,6] Among the promising complex hydrides,[1–3,6] $LiBH_4$ has one of the highest known gravimetric hydrogen densities of 18 mass% and volumetric hydrogen density of 121 kg m^{-3}. It is reversible for hydrogen release and uptake,[7,8] and mainly desorbs hydrogen above ~ 590 K.[9,10] To improve the rather slow kinetics of hydrogen evolution in $LiBH_4$,[7,8] and possibly lower the decomposition/formation temperature, it is mandatory to understand the mechanism involved in the structural changes, formation, and decomposition of the compound.[3] In particular, insight into dynamical properties, which are directly linked to the kinetics of the compound are not well understood in the literature.[11–16]

$LiBH_4$ undergoes a structural phase transition from an orthorhombic low-temperature structure (low-T phase) to a hexagonal high-temperature structure (high-T phase) around 380 K. The melting of the compound occurs at around 550 K. All reported experimental structural studies of $LiBH_4$ and $LiBD_4$ (Refs. 10 and 17–19) have pointed out a dramatic increase in hydrogen or deuterium thermal displacements by almost 2 orders of magnitude from 4 to 400 K. This was attributed to dynamical disorder in the high-T phase.[20,21] However, the microscopic picture of dynamical processes in this compound is still not well understood. It is not only important for the study of structural properties, but it is crucial for the understanding of the slow hydrogen diffusion in $LiBH_4$.[22,23] In order to shed more light on these processes, we performed a combined experimental and theoretical investigation of dynamical properties of $LiBH_4$ and $LiBD_4$.

In the low-T phase, $LiBH_4$ is an ordered quasiharmonic crystal.[18,20,21,24] This allows a straightforward comparison of the structure refined from diffraction data with the one obtained from *ab initio* calculations. In the present paper we report on the experimental low-T structure of $LiBD_4$ at 10 and 302 K obtained from neutron powder diffraction (NPD)

with high signal-to-noise ratio measurements. This data is used in order to refine the best possible experimental structure (i.e., less biased by the covalent nature of the bonds[25] between boron and hydrogen atoms) to be compared with *ab initio* calculations. A particular emphasis is put on the comparison between experimental and theoretical results of thermal motion of the atoms.

Anharmonicities are already noticeable at 302 K in the low-T phase[21,22,24] and increase dramatically above 380 K in the high-T phase where disorder is present.[18,20,21] Therefore for the high-T phase, the refined structure from diffraction data could not be directly compared with the calculated ground-state structure, unless a structural model accounting for disorder and anharmonicities is provided for *ab initio* calculations. A recent attempt for a disordered theoretical model of the high-T phase[16] still needs to be verified experimentally. In the present work, we have investigated the dynamical properties by means of inelastic incoherent neutron scattering (IINS) performed at various temperatures on $LiBH_4$ above and below the structural phase transition. This provides the partial phonon density of states (PDOS) of the hydrogen within the compound. Our measurements of the functional dependence of the PDOS were focused on the low energy lattice vibrations (energies smaller than $\sim$15 meV), giving evidence for temperature-dependent disorder of BH_4 orientations and anharmonicities, independently from any structural model. Our results on external vibrational modes are therefore complementary to previous vibrational spectroscopy study[18,20–22,24] focused on internal vibrational modes of $LiBH_4$.

The excellent agreement found between the experimental and calculated low-T structural properties of $LiBD_4$ allows us to determine from *ab initio* calculations the potential energy landscapes of BH_4 rotations in both high-T and low-T phases, in order to interpret our IINS measurements of hydrogen partial PDOS. The corresponding calculated rotational energy barriers of BH_4 change significantly between the two phases.

II. METHODS

A. Experiment

$LiBH_4$ was purchased from Sigma-Aldrich Chemie GmbH (purity $>$ 95.0%); $LiBD_4$ and $Li(^{11}BH_4)$ were purchased from Katchem Ltd. (produced on special request, purity $>$ 95.0%). All samples were handled under either argon or helium atmosphere.

The NPD measurements were performed on the high-resolution powder diffractometer for thermal neutrons[26] (HRPT) at the Swiss spallation neutron source (SINQ) at the Paul Scherrer Institut (PSI) (Switzerland). Due to the high neutron absorption of natural boron, the powder of $LiBD_4$ was filled into a sealed double walled vanadium cylinder of 9 mm outer diameter, 7 mm inner diameter and 50 mm length. The temperature control of the sample was done by means of a closed-cycle He refrigerator mounted in an evacuated aluminum vessel. For the 10 K measurement, the sample holder was mounted into an additional Al pot for the shielding from radiation heating. Diffraction patterns were recorded with monochromatic neutrons of wavelength of 1.494 Å. The absorption correction coefficient $\mu R = 0.3752$ for the sample has been determined by transmission measurements. The structural refinement was carried out[27] using the program FULLPROF (Ref. 28) (version 3.80).

IINS experiments were performed on $LiBH_4$ on the time-of-flight spectrometer for cold neutrons FOCUS at SINQ at the PSI, and on $Li(^{11}BH_4)$ on the crystal-analyzer inverse-geometry time-of-flight spectrometer TOSCA at the ISIS neutron pulsed source at the Rutherford Appleton Laboratory (United Kingdom). Thanks to the large incoherent cross section of hydrogen, PDOS to 99% represents the partial PDOS of hydrogen. At FOCUS, the measurements were carried out in neutron energy gain mode; therefore at the measured temperatures, energies up to 60 meV were reasonably accessible. The $LiBH_4$ powder was mounted into a flat aluminum sample holder of 1 mm thickness. An incident neutron wavelength of 4 Å was selected. The signal of the empty aluminum sample holder and a flat background have been subtracted with special attention.[29] IINS spectra have been recorded starting from temperatures of 293 and 350 K where the $LiBH_4$ is in the low-T phase, and up to 425 K where the $LiBH_4$ is in the high-T phase. A second spectrum was recorded at 350 K after the measurement done at 425 K in order to check the reversibility of the phase transition (data not shown). Corrections of the measured intensity in order to obtain the PDOS are done for the term $1/\omega$, the polarization factor, the Bose-Einstein statistics for the thermal population, and the Debye-Waller factor. Multiphonon contributions have been estimated and found negligible within the experimental accuracy of the measurement. Although we do have uncertainties in the Debye-Waller factor, the exact background, and absorption issues, the measured spectra are quantitatively correct for energies below 15 meV, and qualitatively correct above 15 meV. These uncertainties are considered in the error bars of Fig. 3. At TOSCA, the IINS spectra have been recorded at 25 K. Since the measurements are carried out in neutron energy loss mode on a sample containing isotope 11 of boron to get rid of the high neutron absorption of natural boron, the analysis of the data is more straightforward. The $Li(^{11}BH_4)$ powder was mounted into a flat aluminum sample holder of 1 mm thickness. The signal of the empty aluminum sample holder and a flat background have been subtracted. The raw data was corrected to obtain $S(Q;\omega)$ using standard routines available at ISIS, which was subsequently corrected for the term $1/\omega$, the polarization factor, and the Debye-Waller factor. Multiphonon contributions were not removed from the data for a qualitative comparison with FOCUS data for energies between 10 and 60 meV.

B. Theory

The structure and the normal mode analysis were calculated within density-functional theory (DFT). The atomic cores were represented by the projected augmented wave (PAW) potentials[30–32] with the electronic configuration $1s^2 2s^1$ for Li, $2s^2 2p^1$ for B, and $1s^1$ for H. The calculations were performed with kinetic energy cutoff of 400 eV and

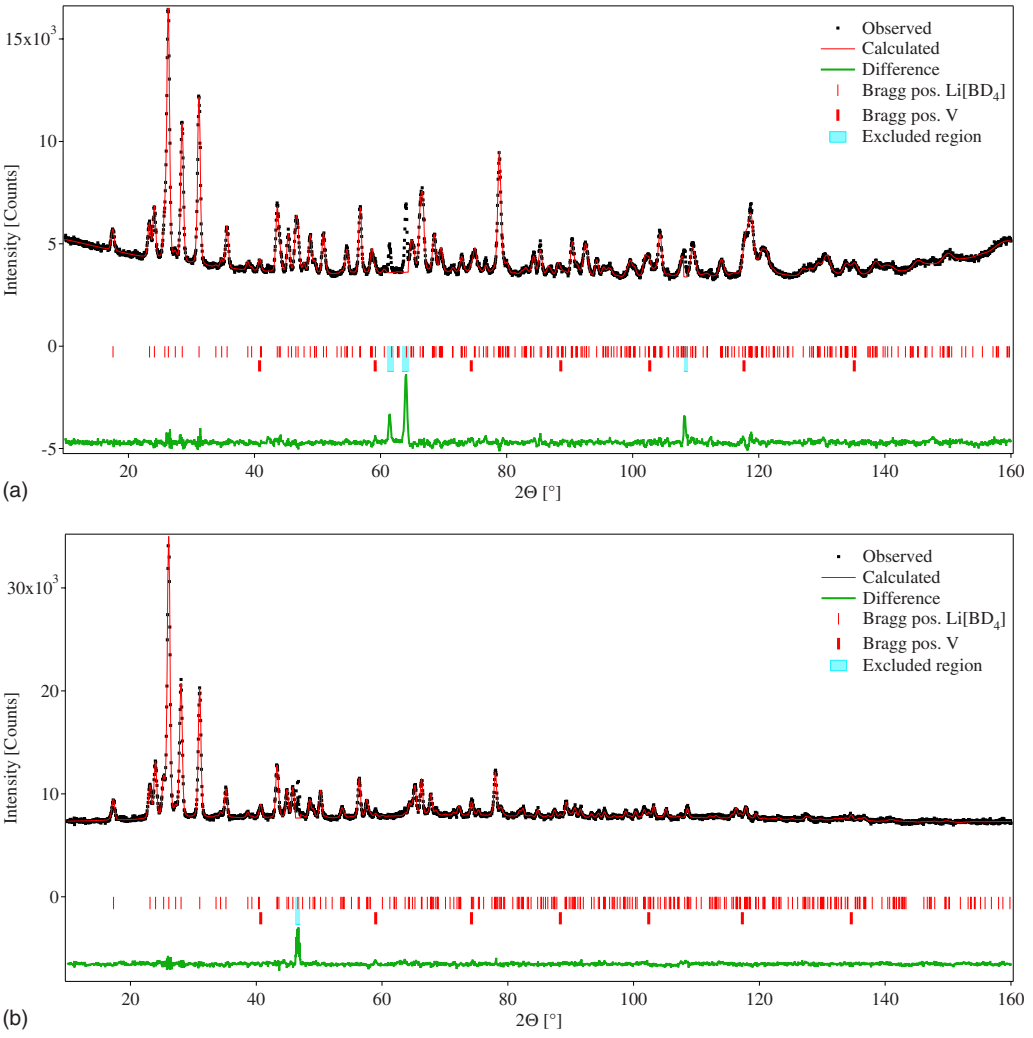

FIG. 1. (Color online) Neutron-diffraction pattern for $LiBD_4$ and results of Rietveld refinement of the structural model at (a) 10 K, (b) 302 K. Excluded regions are, for (a) diffraction peaks arising from the Al thermal shielding not completely removed by the radial collimator, for (b) defect detector wire.

within the generalized gradient approximation (GGA) using the PW91 (Ref. 33) exchange correlation functional. The wave functions were sampled according to the Monkhorst-Pack scheme with a k-points mesh of spacing ≤ 0.05 Å^{-1} for both phases.

The lattice dynamics was determined using the forces acting on atoms in the supercell. The dynamical matrix is constructed from the appropriate set of displacements of the symmetry nonequivalent atoms. The details of the *direct method* are presented elsewhere.[34,35] For calculations of the lattice dynamics and rotational barriers for BH_4 supercells containing 96 atoms were used to assure that rotated BH_4 units do not interact with their periodic images. The thermal displacements were calculated according to the scattering from factors proportional to $\exp[-W_\mu(k)]$, where $W_\mu(k)$ are Debye-Waller factors. The $W_\mu(k)$ depends on the static correlation function $\mathbf{B}(\mu)$ of atomic displacements $U(\mu)$.

$$W_\mu(k) = \pi\mathbf{k} \cdot \mathbf{B}(\mu)(\pi\mathbf{k}),$$

where $\mathbf{B}(\mu)=\langle U_i(\mu)U_j(\mu)\rangle$. In the harmonic approximation correlation function can be expressed via the off-diagonal partial phonon density of states $g(\omega)$:

$$B(\mu) \propto \int d\omega \frac{g_{i,j;\mu}}{\omega}(\omega)\coth\left(\frac{\hbar\omega}{2k_BT}\right).$$

The phonon density of states was calculated for the low-T *Pnma* phase[13,36] of $LiBH_4$.

III. RESULTS AND DISCUSSION

A. Structure and thermal motion of the low-temperature phase of $LiBD_4$

The fits of the NPD patterns at 10 and 302 K resulting from the Rietveld refinement of the orthorhombic structural model with the space group *Pnma* and atomic sites as determined in previous SR-XPD work[10,17,18] are shown in Fig. 1. The refined parameters of the structure are indicated in Table I. The interatomic distances of the BD_4 tetrahedron in the present work (see Table II) are found to be close to the ideal tetrahedral geometry. The relative difference between the longest and shortest interatomic distance is smaller than 4% for B-D bond, and smaller than 3% for the D-D separation. This result is in good agreement with recently reported NPD

TABLE I. Refined structural parameters of the low-T phase of $LiBD_4$. Space group *Pnma* (No. 62), $Z=4$.

Site	$T(K)$	x/a	y/b	z/c	U_{iso} ($Å^2$)
Li/4*c*	10	0.155(3)	0.25	0.109(3)	0.003(12)[a]
	302	0.160(4)	0.25	0.100(9)	0.05(3)[a]
B/4*c*	10	0.307(1)	0.25	0.433(2)	0.0039(15)
	302	0.300(2)	0.25	0.431(3)	0.033(6)[a]
D1/4*c*	10	0.9065(12)	0.25	0.926(2)	0.019(5)[a]
	302	0.901(2)	0.25	0.931(3)	0.060(9)[a]
D2/4*c*	10	0.400(2)	0.25	0.2783(15)	0.025(6)[a]
	302	0.396(3)	0.25	0.286(2)	0.087(15)[a]
D3/8*d*	10	0.2035(9)	0.0281(10)	0.4283(13)	0.027(3)[a]
	302	0.2021(11)	0.0347(16)	0.4265(16)	0.083(6)[a]
$T=10$ K; $a=7.1160(5)$ Å, $b=4.4056(4)$ Å, $c=6.6730(5)$ Å					
$T=302$ K; $a=7.1526(6)$ Å, $b=4.4278(4)$ Å, $c=6.7933(6)$ Å					

[a]Equivalent isotropic temperature factor, calculated from Table III.

TABLE II. Comparison of selected interatomic distance ranges (Å) of BD_4 and BH_4 tetrahedron, for $LiBD_4$ and $LiBH_4$. Difference between the two extreme values of each considered range Δ (%) is indicated.

	Experimental, neutron powder diffraction			
	B-D	D-D	ΔB−D	ΔD−D
10 K[a]	1.18(2)–1.23(2)	1.96(1)–2.00(1)	4.3	2.1
302 K[a]	1.18(2)–1.20(2)	1.91(1)–1.97(2)	1.7	3.2
3.5 K (Ref. 18)	1.208(3)–1.225(6)	1.95–2.00	1.4	2.6
360 K (Ref. 18)	1.184(16)–1.217(15)	1.88–1.97	3.0	4.8
	Experimental, synchrotron x-ray powder diffraction			
	B-H	H-H	ΔB−H	ΔH−H
298 K (Ref. 17)	1.04(2)–1.28(1)	1.73(1)–2.13(2)	23.1	23.1
298 K (Ref. 10)	1.29(4)–1.44(4)	1.29(3)-2.22(4)	11.6	72.1
	Experimental, synchrotron x-ray single crystal diffraction			
	B-H	H-H	ΔB−H	ΔH−H
225 K (Ref. 19)	1.104(11)–1.131(15)		2.4	
	Theoretical			
	B-H	H-H	ΔB−H	ΔH−H
Ref. 13	1.238–1.258	2.002–2.091	1.6	4.4
Ref. 15	1.229–1.258	2.000–2.097	2.4	4.9
Ref. 37	1.228–1.276	1.973–2.090	3.9	5.9
Ref. 37	1.231–1.266	1.986–2.082	2.8	4.8
Ref. 38	1.224–1.23	1.972–2.015	0.5	2.2
Ref. 39	1.216–1.242	1.967–2.033	2.1	3.4
Ref. 40	1.218–1.222	1.960–2.004	0.3	2.2
Ref. 41	1.222–1.228	1.967–2.013	0.5	2.3
0 K (Ref. 41)	1.224–1.229		0.4	
300 K (Ref. 41)	1.226–1.230		0.3	

[a]Present work.

TABLE III. Experimental and calculated anisotropic temperature factors of the low-T phase of $LiBD_4$.

Atom	$T(K)$		U_{11}	U_{22}	U_{33}	U_{12}	U_{13}	U_{23}
Li	10	Exp	0.00(1)	0.01(1)	−0.01(1)	0	−0.008(9)	0
	10	Calc.	0.00872	0.01226	0.01053	0	−0.00053	0
	302	Exp	0.01(2)	0.06(2)	0.08(4)	0	0.01(2)	0
	302	Calc.	0.02186	0.04897	0.04073	0	−0.00314	0
B	10	Exp						
	10	Calc.	0.00633	0.00702	0.00717	0	−0.00076	0
	302	Exp	0.038(6)	0.034(9)	0.027(6)	0	−0.002(9)	0
	302	Calc.	0.02176	0.03708	0.03712	0	−0.00353	0
D1	10	Exp	0.019(3)	0.029(5)	0.011(5)	0	0.005(6)	0
	10	Calc.	0.01813	0.02360	0.01415	0	0.00582	0
	302	Exp	0.068(9)	0.068(9)	0.045(6)	0	0.02(1)	0
	302	Calc.	0.03869	0.06278	0.04146	0	0.00843	0
D2	10	Exp	0.025(6)	0.028(6)	0.022(6)	0	−0.005(5)	0
	10	Calc.	0.01618	0.03632	0.01289	0	0.00297	0
	302	Exp	0.06(1)	0.14(2)	0.06(1)	0	−0.013(9)	0
	302	Calc.	0.03767	0.12839	0.03990	0	0.00072	0
D3	10	Exp	0.021(3)	0.022(3)	0.038(4)	−0.006(3)	−0.010(5)	0.001(4)
	10	Calc.	0.02018	0.01577	0.02996	−0.00713	−0.00500	0.00258
	302	Exp	0.077(6)	0.054(6)	0.116(9)	−0.027(6)	−0.026(9)	0.017(9)
	302	Calc.	0.05074	0.05414	0.09844	−0.01837	−0.02168	0.00910

results,[18] single crystal x-ray diffraction measurements,[19] and results obtained by *ab initio* calculations[13,15,37–41] where the relative differences between the longest and shortest interatomic distances are up to 4% for B-H, and up to 6% for the H-H spacing (see Table II). The apparent shrinking of B-D interatomic distances, apparently shorter of less than 2% at 302 K than at 10 K (see Table II) is essentially due to the imperfect modeling of the thermal libration/bending and riding motion by an ellipsoid distribution in the refinement procedure.[42] After correction[43] of the bond lengths, assuming a riding motion of the hydrogen about the center of mass of a BD_4 unit, when going from 10 to 302 K the tetrahedra show an expansion of less than 1% of the averaged B-D interatomic distances.

A comparison has been done between the refined and *ab initio* calculated matrix elements of the anisotropic temperature factors (see Table III). Qualitatively, the orientation of the experimental and calculated 50% probability ellipsoids of the deuterium atoms at 302 K are in good agreement with little tilt differences for the D1 ellipsoid with respect to the B-D1 bond direction, and D3 ellipsoid with respect to the B-D3 bond direction [see Figs. 2(b) and 2(c)]. For both atoms this is due to the larger difference between the refined and calculated value of the coefficient U_{11} compared to the other coefficients of the temperature factors [see Fig. 2(a)]. The same holds for the difference between the refined and calculated orientation of the ellipsoid of the B atom. The larger difference between the refined and calculated orientation and shape of ellipsoid is found for the Li atom. However the scattering power of this atom for neutron diffraction is very weak, resulting in larger standard deviation of the refined temperature factor parameters compared to the other atoms (see Table III); the experimental accuracy of the temperature factor parameters of Li can therefore not be compared to the ones of D and B atoms. The agreement between experiment and calculation is not only qualitative but also quantitatively consistent as it is shown in Fig. 2(a) for the D3 atom of Table III. Accounting for 3%–5% accuracy for the calculated normal modes frequencies,[24] 13 of the 18 calculated independent coefficients of the temperature factor matrix match the experimental accuracy at 10 K (see Table III). Slightly worse agreement at 302 K indicates deviations from harmonicity (see Table III). Considering the complexity of the structure with 14 independent structural parameters and 19 temperature factor parameters at 10 K (22 at 302 K), possible rotational-translational coupling of the atoms resulting in local anharmonic potentials which is not taken into account in the *ab initio* calculations, and the imperfect modeling of libration/bending thermal motion by ellipsoids for experimental analysis, the agreement between experiment and calculation is surprisingly good.

B. Phonon density of states

From the PDOS shown in Fig. 3(a), the phase transition from the low-T phase to the high-T phase is readily observable with qualitatively different behavior at energies above or below ~15 meV. For energy $E > 15$ meV in Fig. 3(a), two groups of PDOS peaks at $E \sim 25$ meV and $E \sim 48$ meV are pronounced and narrow at 25 K for $Li(^{11}BH_4)$ in Fig. 3(a). They become less pronounced and broaden with increasing temperature in the low-T phase.[44] These two peaks originate from optical modes, which are attributed to lattice vibrations of Li^+ and BH_4^- ions according to *ab initio*

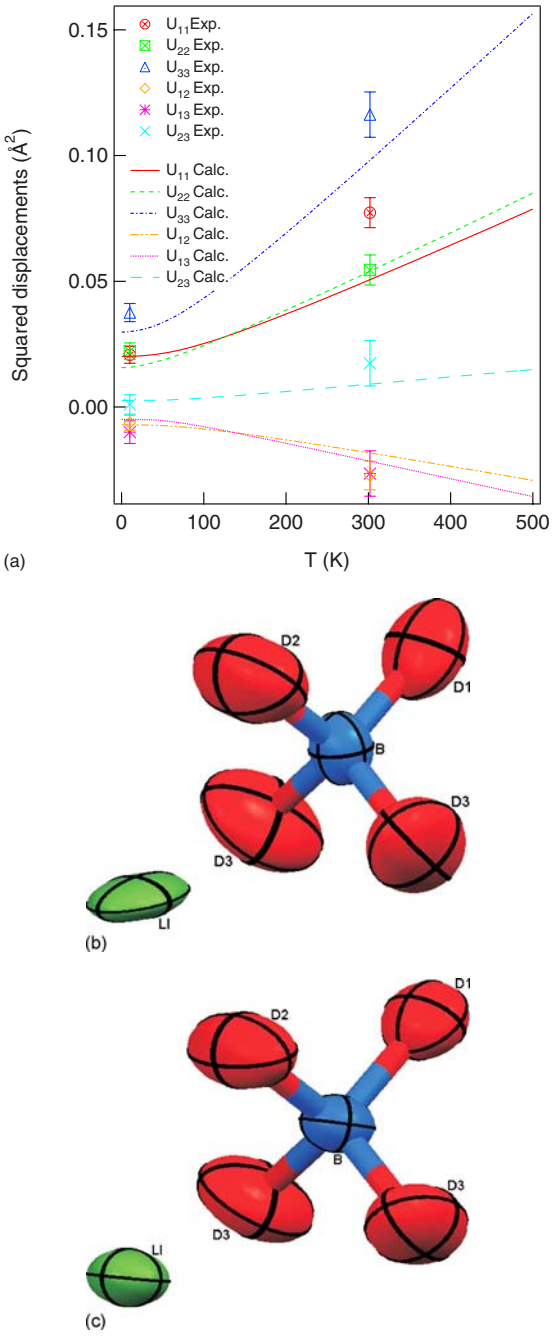

FIG. 2. (Color online) Comparison between experimental and calculated thermal displacements for $LiBD_4$. (a) Experimental and calculated elements of the thermal displacements matrix for the D3 atom as a function of the temperature; (b) experimental 50% probability ellipsoids at 302 K, (c) calculated 50% probability ellipsoids at 300 K.

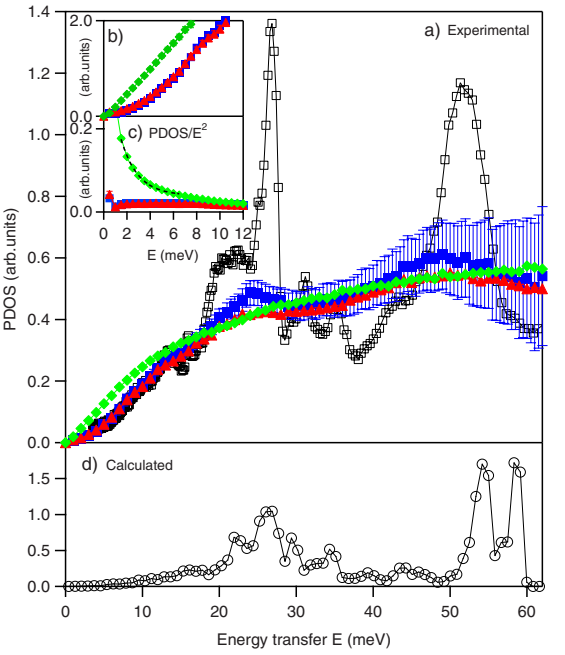

FIG. 3. (Color online) (a) PDOS of hydrogen for $LiBH_4$ in the low-T phase at 295 K (blue squares) and 350 K (red triangles), in the high-T phase at 425 K (green lozenges), and for $Li(^{11}BH_4)$ in the low-T phase at 25 K (black empty squares). Representative errors bars are only shown for the data giving the biggest error bars, i.e., at 295 K. (b) Enlargement for energies below 12 meV of the PDOS of hydrogen for $LiBH_4$ shown in (a). (c) $PDOS/E^2$ in order to emphasis the excess of low-E density of states at 425 K (green lozenges) compared to the density of states at 295 K (blue squares) and 350 K (red triangles), the black dotted line shows an exponential fit of the low energy transfer part of the data measured at 425 K. (d) Theoretical calculation of partial PDOS of hydrogen for $LiBH_4$.

calculations. Figure 3(d) represents the calculation of the partial hydrogen PDOS caused by the hydrogen density following the overall BH_4 complex vibrations. Similar peak broadening was reported in the literature and was either attributed to large vibrational amplitudes,[20] or to phonon interactions.[24,45] This was recently extensively discussed for a series of Raman measurements[24] on $LiBH_4$ where for some peaks a broadening of a factor ~10 of the full width at half maximum (FWHM) between 5 and 300 K was observed. The complete disappearance of distinct peaks in the PDOS of the high-T phase is surprising though. For $E<15$ meV, a specific feature of the high-T phase compared to the low-T phase is the increased PDOS, indicative of acoustic bands that are lower in energy than found for the low-T phase. The PDOS of the low-T phase depends quadratically on the phonon energy as expected by the Debye theory for acoustic vibrations in crystalline solids [see Fig. 3(b)]. This feature is basically temperature independent for energies below 15 meV. Interestingly, the high-T phase shows a linear dependence of the PDOS as a function of the phonon energy [see Fig. 3(b)]. Compared to the PDOS given by the Debye theory, the excess of density of states of the high-T phase reveals a high lattice anharmonicity and it is a characteristic feature of glasses and disordered systems.[46–48] In the representation of the reduced quantity $PDOS/E^2$ with respect to E [see Fig. 3(c)], this characteristic excess of PDOS is more clearly identified by a maximum in $PDOS/E^2$ called boson peak[46–48] (usually below ~8 meV). Figure 3(c) shows that $PDOS/E^2$ for the low-T phase at 295 and 350 K is nearly constant as function of energy as expected for an ordered quasiharmonic crystal. Contrarily, for the high-T phase $PDOS/E^2$ at 425 K exhibits an exponential dependence with respect to E [fitted by the black dotted line in Fig. 3(c)] indicating a disorder in the high-T phase similar to the one

encountered in glasses and disordered systems.[49] This observation suggests large disorder of the BH_4 tetrahedra in the structure. Quasielastic contributions are significant in our data for $E<2$ meV. Even if we could not explicitly identify a maximum of PDOS$/E^2$ at 425 K (Boson peak broadens with increasing temperature and disappears close to the glass-liquid transition[49]), from the exponential fit [see Fig. 3(c)] the maximum of the boson peak is expected to be at $E=2.9(3)$meV.

C. Calculation of the rotational energy barriers of a BH_4 unit in $LiBH_4$

Strengthened by the agreement between experimental and calculated structure and temperature factors, we have calculated potential energy barriers for rotation of BH_4 units in $LiBH_4$. Potential energy landscapes shed more light on the order and disorder features of BH_4 in $LiBH_4$ (resp. BD_4 in $LiBD_4$). The rotational barriers were calculated for the structure of the low-T phase with space group *Pnma* and with space group $P6_3mc$ for the high-T phase.[17] No atomic relaxation was performed during rotation, such that the potential energy landscapes presented in Fig. 4 render adiabatic barriers. Since the description of BH_4 orientation in Cartesian three-dimensional space requires a three parameter space based on Euler angles, we have decided to simplify the problem in order to represent it in two dimensions. Two rotational axes were chosen for each structure. One of the axes is related to C_2 pseudosymmetry of BH_4, the second one is the C_3 symmetry of the molecule, as shown in Fig. 4(a). Potential energy surfaces were calculated for rotation around C_2 axis, and subsequent rotation around C_3 axis. One has to keep in mind that group of rotations is not commutative, thus rotation first around C_3 than around C_2 would result in different cross sections. The potential energy landscape is presented in Figs. 4(b) and 4(c). Thanks to the almost perfect tetrahedral shape of the BH_4 units, the intersection of the vertical, horizontal, and frame lines of Figs. 4(b) and 4(c) correspond in good approximation to equivalent orientations of the BH_4 unit and zero energy level is defined for $C_2=C_3=0$. One can see in Fig. 4(b) for the low-T *Pnma* phase that the orientation of a BH_4 unit is fairly localized by the energy minima and coincide with the equivalent orientations of the BH_4 unit, i.e., equivalent orientations correspond to equilibrium orientations of the BH_4 units, and the barriers between minima are higher than 0.6 eV. The potential energy landscape is significantly different for the high-T $P6_3mc$ phase. One can see in Fig. 4(c) that some equivalent orientations are surrounded by regions of lower energy. These orientations are located in fact on saddle points; therefore the energy minima of the energy landscape do not coincide with the equivalent orientations of the BH_4 unit. This is a simple visualization of the fact that this structure is not stable in this symmetry, unless it is stabilized by entropy (this was previously reported in the literature by unphysical imaginary phonon modes in *ab initio* calculations[13,15]). The potential seen by rotating BH_4 molecule is very shallow when compared to low-T phase, and localized minima are not present. In fact shallow energy valleys traverse whole energy landscape, barriers between

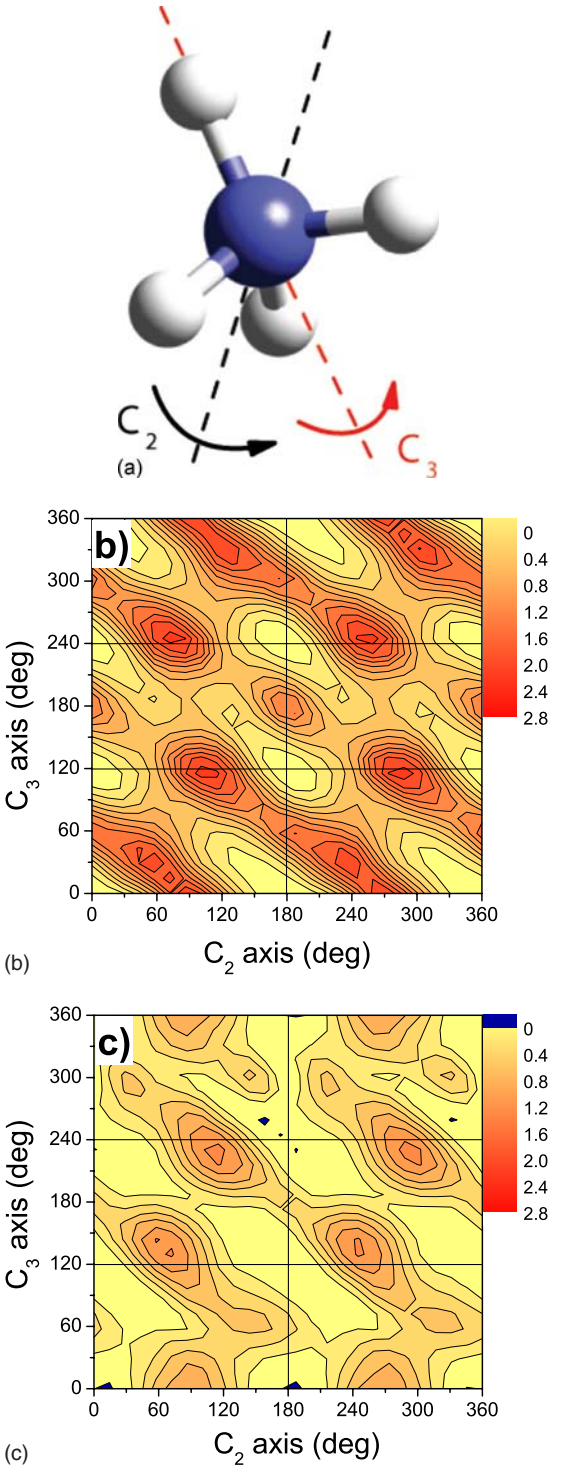

FIG. 4. (Color online) Calculation of the rotational energy barriers of the BH_4 tetrahedra in $LiBH_4$. (a) Rotation axis C_2 and C_3 used for the description of all the orientations of the tetrahedra. Potential energy surface calculated along the two axis C_2 and C_3 (b) for *Pnma* space group, (c) for $P6_3mc$ space group.

minima are ~0.2 eV. In recent Raman measurements[21] on $LiBH_4$, two types of external thermal motion of the BH_4 were suggested in order to fit the linewidth of the BH_4 bands for the high-T phase: a reorientation barrier of 0.05(5) eV around the C_3 axis of the BH_4 units and a barrier correspond-

ing to orientational disorder between axial and peripheral directions of the BH_4 units of 0.6(3) eV. Unless their significant relative uncertainty, they are in agreement with the calculated energy barriers. The calculated rotational energy landscapes clarify this situation and the origin of disorder in this phase. On Fig. 4(c), the lowest energy barrier is indeed found for the rotation barrier about C_3 axis (for $C_2 = 0°, 180°, 360°$) as well as for orientations corresponding to the extremities of the elongated energy valleys. Large thermal displacements are also to be expected within the flat energy valley. In order to evaluate the temperature dependence of the reorientation rate of the BH_4 units, the following Arrhenius equation was considered:

$$A \exp\left(\frac{-\Delta E}{kT}\right),$$

where ΔE is the reorientation barrier and $A = 10^{12}$ Hz the typical prefactor for thermally activated diffusion.[50] Small barriers ΔE lower than ~ 0.2 eV indicate that above the temperature of the phase transition ($kT = 0.033$ eV), the reorientation time scale will be of the order GHz to THz. Thus, orientation of a single BH_4 unit cannot be precisely defined; orientational disorder must be present in at least four broad directions with similar probability (all the barriers are ~ 0.2 eV, two of them corresponding to rotational disorder about C_3 axis). By contrast, for the low-T phase, the reorientation time scale will be of the order Hz at room temperature ($kT = 0.025$ eV) and kHz at the temperature of the phase transition. That is a minor disorder, slightly increasing with temperature, is expected in this phase. These calculations corroborate our IINS results, namely fairly ordered BH_4 units in the low-T phase whose orientations are defined by rather deep potential minima [in agreement with the PDOS typical for a crystalline solid shown for low-T phase in Fig. 3(b)]. The highly disordered orientation of the BH_4 units in the high-T phase whose orientations are roughly defined by shallow anharmonic potentials give rise to the PDOS typical for highly disordered systems shown for high-T phase in Fig. 3(b).

IV. CONCLUSION

In the present paper, we report experimental and theoretical studies of dynamical properties of $LiBH_4$ and $LiBD_4$. By means of neutron diffraction, we found an almost ideal tetrahedral geometry of BD_4 ions at 10 and 302 K (difference between shortest and longest interatomic distances is less than 4% for B-D bond, and less than 3% for D-D bond), close to the calculated geometry. Furthermore, excellent agreement was found between experimental and calculated anisotropic temperature factors of individual atoms. The partial phonon density of states of hydrogen has been measured by inelastic incoherent neutron scattering in the low-temperature phase (at 25, 293, and 350 K) and in the high-temperature phase (at 425 K). For energies below 15 meV, an increased phonon density of states is observed in the high-temperature phase. While for the low temperature, a quadratic dependence of the density of states on energy, characteristic for quasiharmonic ordered crystal, is observed. This gives a direct evidence for disorder in the high-temperature phase of $LiBH_4$ of the hydrogen sublattice which can originate from orientational disorder of BH_4 units. Calculated potential energy landscape for rotation of BH_4 indicates that fairly localized minima and barriers higher than 0.6 eV exist in the low-temperature phase, i.e., ordered BH_4 ions. The high-temperature structure with $P6_3mc$ symmetry shows shallow barriers of ~ 0.2 eV without distinct energy minima, i.e., orientation of a single BH_4 unit cannot be precisely defined, corroborating the thermal displacements observed in diffraction studies and high disorder of BH_4 ions deduced from experimental partial phonon density of states in the present work.

ACKNOWLEDGMENTS

CPU time allocation at CSCS supercomputer center (Manno) is kindly acknowledged. This work was partially based on experiments performed at the Swiss spallation neutron source SINQ, Paul Scherrer Institut, Villigen, Switzerland. Support from the TOSCA team instrument (ISIS, United Kingdom) is gratefully acknowledged. Financial support by the Swiss National Science Foundation (Schweizerischer Nationalfonds, SNF), Projects No. 200021-111683 and 200020-115875, is gratefully acknowledged. Financial support by the European Commission DG Research (Contract No. SES6-2006-518271/NESSHY) and the Helmholtz Initiative "FuncHy" is gratefully acknowledged.

*University of Fribourg, Physics Department, CH-1700 Fribourg, Switzerland; florian.buchter@empa.ch
†University of Fribourg, Physics Department, CH-1700 Fribourg, Switzerland

[1] A. Züttel, A. Borgschulte, and L. Schlapbach, *Hydrogen as a Future Energy Carrier* (Wiley, New York, 2008).
[2] S. Orimo, Y. Nakamori, J. Eliseo, A. Züttel, and C. M. Jensen, Chem. Rev. (Washington, D.C.) **107**, 4111 (2007).
[3] A. Züttel, A. Borgschulte, and S. Orimo, Scr. Mater. **56**, 823 (2007).
[4] B. Bogdanovic and M. Schwickardi, J. Alloys Compd. **253-254**, 1 (1997).
[5] D. J. Siegel, C. Wolverton, and V. Ozoliņš, Phys. Rev. B **76**, 134102 (2007).
[6] C. Wolverton, D. J. Siegel, A. R. Akbarzadeh, and V. Ozoliınš, J. Phys.: Condens. Matter **20**, 064228 (2008).
[7] Ph. Mauron, F. Buchter, O. Friedrichs, A. Remhof, M. Bielmann, C. N. Zwicky, and A. Züttel, J. Phys. Chem. B **112**, 906 (2008).
[8] O. Friedrichs, F. Buchter, A. Borgschulte, A. Remhof, C. N. Zwicky, Ph. Mauron, M. Bielmann, and A. Züttel, Acta Mater. **56**, 949 (2008).
[9] A. Züttel, P. Wenger, S. Rentsch, P. Sudan, Ph. Mauron, and Ch.

Emmenegger, J. Power Sources **118**, 1 (2003).
[10] A. Züttel, S. Rentsch, P. Fisher, P. Wenger, P. Sudan, Ph. Mauron, and Ch. Emmenegger, J. Alloys Compd. **356-357**, 515 (2003).
[11] E. M. Fedneva, V. L. Alpatova, and V. I. Mikheeva, Russ. J. Inorg. Chem. **9**, 826 (1964).
[12] D. S. Stasinevich and G. A. Egorenko, Russ. J. Inorg. Chem. **13**, 341 (1968).
[13] Z. Łodziana and T. Vegge, Phys. Rev. Lett. **93**, 145501 (2004).
[14] A. Rebei and J. Hohlfeld, Phys. Rev. Lett. **97**, 117601 (2006).
[15] K. Miwa, N. Ohba, S. I. Towata, Y. Nakamori, and S. I. Orimo, Phys. Rev. B **69**, 245120 (2004).
[16] N. A. Zarkevich and D. D. Johnson, Phys. Rev. Lett. **100**, 040602 (2008).
[17] J-Ph. Soulié, G. Renaudin, R. Černý, and K. Yvon, J. Alloys Compd. **346**, 200 (2002).
[18] M. Hartman, J. Rush, T. Udovic, R. Bowman, Jr., and Son-Jong Hwang, J. Solid State Chem. **180**, 1298 (2007).
[19] Y. Filinchuk, D. Chernyshov, and R. Černý, J. Phys. Chem. C **112**, 10579 (2008).
[20] S. Gomes, H. Hagemann, and K. Yvon, J. Alloys Compd. **346**, 206 (2002).
[21] H. Hagemann, S. Gomes, G. Renaudin, and K. Yvon, J. Alloys Compd. **363**, 126 (2004).
[22] A. Borgschulte, A. Züttel, P. Hug, A.-M. Racu, and J. Schoenes, J. Phys. Chem. A **112**, 4749 (2008).
[23] M. Matsuo, Y. Nakamori, S. Orimo, H. Maekawa, and H. Takamura, Appl. Phys. Lett. **91**, 224103 (2007).
[24] A. M. Racu, Z. Łodziana, A. Borgschulte, A. Züttel, and J. Schoenes, J. Phys. Chem. A (to be published).
[25] The distortion of the BH_4 tetrahedron determined with SR-XPD previously reported (Refs. 10 and 17) is proposed to be due to the covalent nature of the bond between B and H atoms. X rays interact with electrons in the solid that are significantly delocalized for light covalent compounds (especially valence electrons), while neutrons interact with the nuclei, thus yielding atomic positions closer to the center of mass of the atoms. The limited number of measured diffraction peaks in the former SR-XPD experiments [$\approx$50 diffractions peaks (Refs. 10 and 17] could explain the distorted refined BH_4 since the x-ray diffraction peaks of low 2θ angle are more affected by the deformation of the outermost electron density of the atoms involved in a covalent bond (Ref. 51).
[26] P. Fischer, G. Frey, M. Koch, M. Könnecke, V. Pomjakushin, J. Schefer, R. Thut, N. Schlumpf, R. Bürge, U. Greuter, S. Bondt, and E. Berruyer, Physica B (Amsterdam) **276-278**, 146 (2000).
[27] Two phases, $LiBD_4$ and V, are considered in the refinement. Scattering length from the FullProf library were used. Thomson-Cox-Hastings modified pseudo-Voigt profile function was used, and a 12-coefficient Fourier-cosine series was used for modeling the background. The refinement of the $LiBD_4$ structure at 10 K was done using 3 unit cell parameters, 11 atomic positions, 18 anisotropic temperature factor coefficients for Li and D atoms, 1 isotropic temperature factor for B atom, 6 profile parameters and 1 zero shift parameter. The refinement of the $LiBD_4$ structure at 302 K was done using 3 unit cell parameters, 11 atomic positions, 22 anisotropic temperature factor coefficients, 6 profile parameters and 1 zero shift parameter.
[28] J. Rodríguez-Carvajal, Physica B (Amsterdam) **192**, 55 (1993).
[29] To take into account for the huge neutron absorption of natural boron contained in the sample, the empty sample holder signal is subtracted from the signal measured with the sample only for the detectors which are not shielded during the measurement with the sample. This is done by cutting the empty sample holder signal for the detectors with an angle $2\theta < 45°$, since the sample was mounted with an angle of 45° with respect to the incident beam in order to improve the intensity of the backscattering signal.
[30] P. E. Blöchl, Phys. Rev. B **50**, 17953 (1994).
[31] G. Kresse and J. Furthmüller, Comput. Mater. Sci. **6**, 15 (1996).
[32] L. Bellaiche and K. Kunc, Phys. Rev. B **55**, 5006 (1997).
[33] J. P. Perdew, J. A. Chevary, S. H. Vosko, K. A. Jackson, M. R. Pederson, D. J. Singh, and C. Fiolhais, Phys. Rev. B **46**, 6671 (1992).
[34] K. Parlinski, Z-.Q. Li, and Y. Kawazoe, Phys. Rev. Lett. **78**, 4063 (1997).
[35] Z. Łodziana and K. Parlinski, Phys. Rev. B **67**, 174106 (2003).
[36] Z. Łodziana and T. Vegge, in *Materials for Hydrogen Storage–2004*, MRS Symposia Proceedings No. 837 (Materials Research Society, Pittsburgh, 2004), p. N 1.7.
[37] T. Frankcombe, G. Kroes, and A. Züttel, Chem. Phys. Lett. **405**, 73 (2005).
[38] Q. F. Ge, J. Phys. Chem. A **108**, 8682 (2004).
[39] J. Kang, S. Kim, R. Muller, and W. Goddard III, Appl. Phys. Lett. **87**, 111904 (2005).
[40] P. Vajeeston, P. Ravindran, A. Kjekshus, and H. Fjellvag, J. Alloys Compd. **387**, 97 (2005).
[41] T. J. Frankcombe and G. J. Kroes, Phys. Rev. B **73**, 174302 (2006).
[42] B. T. Willis and A. W. Pryor, *Thermal Vibrations in Crystallography* (Cambridge University Press, Cambridge, 1975).
[43] W. R. Busing and H. A. Levy, Acta Crystallogr. **17**, 142 (1964).
[44] The observed peak broadening is much larger than the instrumental resolution.
[45] D. M. Trots, A. N. Skomorokhov, M. Knapp, and H. Fuess, Eur. Phys. J. B **51**, 507 (2006).
[46] S. R. Elliott, *Physics of Amorphous Materials* (Longmans, Green, 1990).
[47] G. Parisi, J. Phys.: Condens. Matter **15**, S765 (2003).
[48] S. Ciliberti, T. S. Grigera, V. Martìn-Mayor, G. Parisi, and P. Verrochio, in *SLOW DYNAMICS IN COMPLEX SYSTEMS: 3rd International Symposium on Slow Dynamics in Complex Systems*, edited by M. Tokuyama and I. Oppenheim, AIP Conf. Proc. No. 708 (AIP, Melville, NY, 2004), p. 565.
[49] A. I. Chumakov, I. Sergueev, U. van Bürck, W. Schirmacher, T. Asthalter, R. Rüffer, O. Leupold, and W. Petry, Phys. Rev. Lett. **92**, 245508 (2004).
[50] G. L. Kellogg, Surf. Sci. Rep. **21**, 1 (1994).
[51] P. Coppens, *X-Ray Charge Densities and Chemical Bonding, International Union of Crystallography* (Oxford University Press, New York, 1997).